ACS OMEGA

http://pubs.acs.org/journal/acsodf

Article

# Iron-Intercalated Zirconium Diselenide Thin Films from the Low-Pressure Chemical Vapor Deposition of $[Fe(\eta^5\text{-}C_5H_4Se)_2Zr(\eta^5\text{-}C_5H_5)_2]_2$

Clara Sanchez-Perez, Caroline E. Knapp, Ross H. Colman, Carlos Sotelo-Vazquez, Sanjayan Sathasivam, Raija Oilunkaniemi, Risto S. Laitinen,* and Claire J. Carmalt*

Cite This: https://dx.doi.org/10.1021/acsomega.0c00413

Read Online

ACCESS | Metrics & More | Article Recommendations | Supporting Information

**ABSTRACT:** Transition metal chalcogenide thin films of the type $Fe_xZrSe_2$ have applications in electronic devices, but their use is limited by current synthetic techniques. Here, we demonstrate the synthesis and characterization of Fe-intercalated $ZrSe_2$ thin films on quartz substrates using the low-pressure chemical vapor deposition of the single-source precursor $[Fe(\eta^5\text{-}C_5H_4Se)_2Zr(\eta^5\text{-}C_5H_5)_2]_2$. Powder X-ray diffraction of the film scraping and subsequent Rietveld refinement of the data showed the successful synthesis of the $Fe_{0.14}ZrSe_2$ phase, along with secondary phases of FeSe and $ZrO_2$. Upon intercalation, a small optical band gap enhancement ($E_{g(direct)}^{opt}$ = 1.72 eV) is detected in comparison with that of the host material.

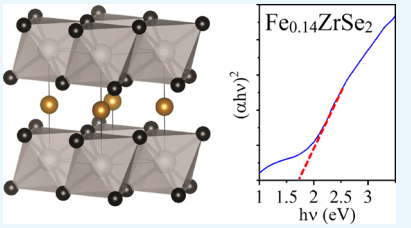


## INTRODUCTION

Transition metal dichalcogenide (TMD) layered materials have attracted a great deal of interest due to their unique physical properties beyond those of graphene as they are generally non-toxic and abundant, have energy band gaps well-suited for solar energy conversion and high absorption coefficients in the visible range.[1] TMDs of group 4, 5, and 6 metals are diamagnetic semiconductors with band gap values in the range of 0.2−2.0 eV.[2,3] They have received special interest due to their mechanical and electrical anisotropy[2,4] and charge density wave transitions, related to their structures being composed of layers of $TX_2$ (T = transition metal; X = chalcogen) stack along the *c* axis *via* van der Waals forces.[2,5] Zirconium diselenide ($ZrSe_2$) in particular has attracted considerable attention in the fields of physics, chemistry, and materials due to their unique structural, optical,[6,7] and electronic properties. While the use of $ZrSe_2$ in secondary lithium batteries confronts electrochemical challenges,[8,9] it shows many potential applications as working materials in photovoltaic solar cells[10,11] given that its band gap falls in the visible region of the electromagnetic spectrum ($E_{g(indirect)}^{opt}$ = 1.20 eV; $E_{g(direct)}^{opt}$ = 1.61 eV).[6,12] Group 4 ($d^0$) TMD such as $ZrSe_2$ stabilize 1T structures under normal conditions, with a $CdI_2$ (HCP packing) structure and $P\bar{3}m1$ symmetry.[13] This structure type allows the intercalation of small molecules or atoms (electron donors) between $TX_2$ layers,[5] which transfer electrons from the intercalate to the transition metal unoccupied d band.[4] The intercalation of electron-donating atoms in TMD layered materials can be used to modulate the intrinsic physical properties of the host material[4] that result into band gap changes,[14] phase transition processes,[15,16] and development of magnetic and superconducting behaviors.[2,4,5] In the case of $ZrSe_2$ different alkali,[17] transition[15,16,18,19] and post-transition[20] metals have been intercalated to modulate electronic states and dramatically change the opto-electronic and magnetic properties of the host material. In some cases, a relatively low intercalation produces a significant change while virtually retaining the host structure.[13]

$ZrSe_2$ is one of the few metal chalcogenide hosts able to accommodate Fe both into tetrahedral and octahedral sites between layers,[15] with the Fe relative site distribution dependent on the total amount of Fe and the thermal treatment of the material.[16] At intercalation levels $x$ = 0−0.16, a semiconducting $Fe_xZrSe_2$ phase exists with a trigonal structure $P\bar{3}m1$ derived from that of $ZrSe_2$, intermediate between 1T-$CdI_2$ and NiAs types, and at the critical iron concentration of $x$ = 0.41, the material becomes metallic.[13] Hybridization of the 3d bands of Zr and Fe, along with the overlap of their $d_z^2$ electron shells along the *c* axis leads to a covalent interaction between $ZrSe_2$ layers, ultimately affecting the unit cell lattice constants.[19,21] As the intercalation of transition metals in TMD 1T polymorphs donates free carriers to their empty conduction band, increasing their conductivity,[4,22] they can be selectively used to fine-tune the electric, magnetic, optical, and structural properties of the host materials in a controllable way to fit application requirements.[5]

$ZrSe_2$ and $Fe_xZrSe_2$ materials have traditionally been synthesized from high-purity elements[8,13,15,16,23] (long multi-step processes at high temperatures) or chemical vapor

Received: January 29, 2020
Accepted: June 10, 2020

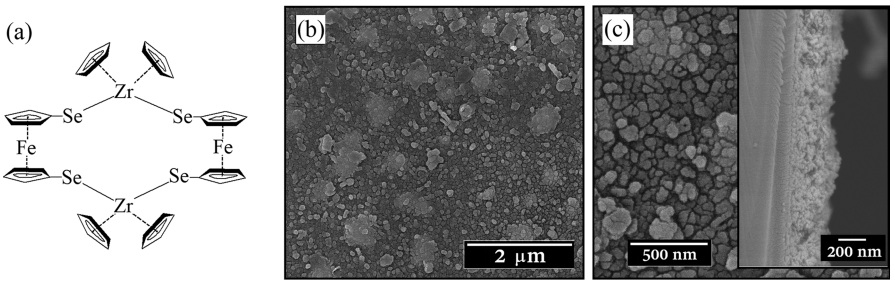


**Figure 1.** (a) Schematic representation of precursor $[Fe(\eta^5\text{-}C_5H_4Se)_2Zr(\eta^5\text{-}C_5H_5)_2]_2$ used in LPCVD to grow $Fe_xZrSe_2$ thin films. (b, c) SEM images of the thin film at x10k and x40k magnification, respectively. The inset shows the cross-sectional image to reveal a film thickness of *ca.* 300 nm.

transport reactions,[2,6,8,17,24] mainly as single crystals and, in few cases, in nanoparticle form.[25,26] The synthesis of $ZrSe_2$ thin films has been mainly reported *via* electrodeposition methods,[11,27−29] although the synthesis using MBE[30] and CVD[31] has been reported as an alternative for the requirement of conductive substrates, which can be problematic for device applications. The absence of studies of $Fe_xZrSe_2$ in thin film form is likely due to the lack of precursors for these ternary systems using established deposition methods. Low-pressure chemical vapor deposition (LPCVD) of organometallic precursors appears to be a suitable alternative due to its versatility toward the use of alternative air/moisture-sensitive precursors. This method allows growth of high-quality thin films from volatile, temperature-sensitive reagents and has been used extensively in the past decade for the synthesis of thin films of functional materials, many of them metal selenides.[32−34] In the present paper, we investigate the ability of single-source precursor $[Fe(\eta^5\text{-}C_5H_4Se)_2Zr(\eta^5\text{-}C_5H_5)_2]_2$ (**1**) to successfully generate thin films of Fe-intercalated $ZrSe_2$ (i.e., $Fe_xZrSe_2$) using a convenient single-step deposition process *via* LPCVD and record the optical band gap shift resultant from the intercalation.

## RESULTS AND DISCUSSION

Following our previous work on $Fe_xTiSe_2$ thin films *via* LPCVD from the single-source precursor $[Fe(\eta^5\text{-}C_5H_4Se)_2Ti(\eta^5\text{-}C_5H_5)_2]_2$,[34] $Fe_xZrSe_2$ thin film synthesis from $[Fe(\eta^5\text{-}C_5H_4Se)_2Zr(\eta^5\text{-}C_5H_5)_2]_2$ (**1**) (Figure 1a) was investigated.

The highly reflective and black $Fe_xZrSe_2$ films grown using LPCVD under a dynamic pressure of $10^{-1}$ Torr at 1000 °C were air/moisture-sensitive but highly robust with complete coverage of the quartz substrate. Scanning electron microscopy (SEM) analysis of the films showed that the surface morphology consisted of irregular quasi-spherical grains uniformly distributed over the entire surface of the substrate (Figure 1b,c), in a similar way as previously reported for $ZrSe_2$ thin films.[28] The film is fairly densely packed both laterally and vertically, and the cross-sectional SEM imaging of the film showed a thickness of ∼300 nm (Figure 1c, inset).

Glancing-angle X-ray diffraction (XRD) analysis of the $Fe_xZrSe_2$ films was not possible due to fluorescence of iron in the presence of the Cu $K_{\alpha1}$ radiation. Therefore, the films were scraped off to give powders that were then analyzed *via* powder XRD (PXRD) using a Mo$K_{\alpha1}$ source in order to obtain patterns with reduced fluorescence effects. Rietveld refinement, carried out on the data to determine the crystallographic properties of the films (Figure 2), showed that layered $ZrSe_2$ with intercalated Fe had indeed been formed.

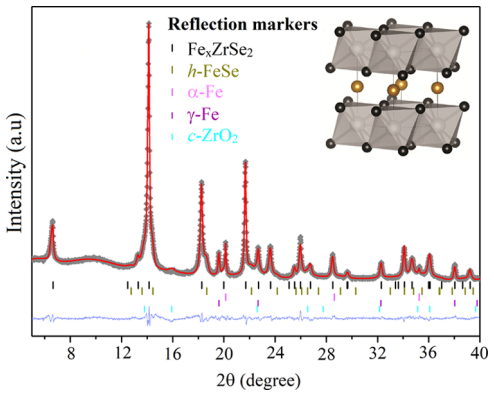


**Figure 2.** Rietveld refined powder diffraction data (crosses), fit (red line), difference curve (shifted blue line), and reflection markers for all phases (ticks).[13,35−38] Structural analysis was performed using the GSAS package,[39] and reference patterns from ICSD were used. Embedded in the right corner is an image of the $Fe_xZrSe_2$ structure drawn from structurally refined PXRD data using VESTA,[40] showing Zr and Se atoms (gray and black spheres) making up edge-linked layers of $ZrSe_2$ octahedra in the *ab* plane, separated by Fe atoms (gold spheres) randomly occupying the octahedral vacancies within the van der Waals gap with a refined occupancy of ∼14%.

However, small additional crystalline secondary phases of *α*- and *γ*-Fe, hexagonal FeSe, and $ZrO_2$ were also observed. The secondary phase formation is likely due to a combination of post-deposition oxidation (semi-amorphous nature of $ZrO_2$) during post-deposition film handling and due to possible Fe saturation in between the layers (e.g., FeSe and *α*- and *γ*-Fe) (Figure 2). The parent compound $ZrSe_2$ is known to crystallize in the $CdI_2$ structure type with $P\bar{3}m1$ symmetry, identical to that of $TiSe_2$, as shown from the Rietveld analysis. The structure exists as sheets of Zr atoms, octahedrally coordinated by Se atoms, with each Se bonded to three Zr atoms. The two-dimensional $ZrSe_2$ sheets are AA stacked and weakly bound, with the space between sheets commonly referred to as the van der Waals gap. Structural modifications to the parent $ZrSe_2$ lattice upon the intercalation of variable amounts of Fe within the van der Waals gap have previously shown a change of symmetry due to intercalant site ordering at $x \geq 0.41$ (in $Fe_xZrSe_2$), along with the onset of metallicity.[13] In addition to the impurity phases, the two-dimensionality of the material (stacked layers) leads to the expected preferred orientation effects that were modeled within the refinement (see Supporting Information, Table S1 and Figure S1 for further refinement details). The $Fe_xZrSe_2$ material shows no sign of superstructure and was best modeled using the parent $P\bar{3}m1$ space group, indicating no site ordering of intercalated Fe


https://dx.doi.org/10.1021/acsomega.0c00413
ACS Omega XXXX, XXX, XXX−XXX

atoms and a value of the intercalation of $x < 0.41$.[13] Changes in lattice parameters are often used as an indication of intercalation in transition metal dichalcogenides. The interlayer distance is expectedly found to increase upon the intercalation of transition metals, resulting in an increase of the $c$ lattice parameter (e.g., $Fe_xZrSe_2$[13] or $Cu_xZrSe_2$[19]).

Our observed interlayer lattice parameter, $c = 6.1336(3)$ Å, lies between the values reported for $x = 0.18$ ($c = 6.138(2)$ Å) and $x = 0.465$ ($c/2 = 6.011(1)$ Å).[13] Care must be taken when interpreting this effect, however, due to the possibility of non-stoichiometric Zr:Se ratios. Non-stoichiometry of Zr:Se has been seen to significantly influence both the lattice parameter and electron transport properties.[41] Our observed $c$ lattice parameter is larger than the reported value for near-stoichiometric $ZrSe_{1.937}$ ($c = 6.1297(9)$ Å) while being only slightly smaller than Se-deficient $ZrSe_{1.851}$ ($c = 6.1510(9)$ Å), complicating interpretation as evidence of intercalation.[41] While the refinement of structural details has been attempted, reported errors on the values obtained may vary due to the data quality and the modeling of preferred orientation and additional phases. The refinements were improved upon the introduction of Fe within the van der Waals gap modeled in an identical manner to that previously seen in $Fe_xZrSe_2$, placing Fe directly between the layers on the 1b Wyckoff site (0, 0, and 1/2) and refined to a value of $x = 13.5(5)\%$, suggesting $Fe_{0.14}ZrSe_2$ (Table 1).

**Table 1. Selected Parameters from Rietveld Refinements of Powder X-ray Diffraction Data**

| target composition | $Fe_xZrSe_2$ |
|---|---|
| space group | $P\bar{3}m1$ |
| lattice parameters (Å) | $a = 3.77239(6)$; $c = 6.1336(3)$ |
| Fe fractional occupancy, $x$ | 0.135(5) |
| $Fe_xZrSe_2$ phase fraction (wt %) | 61.9(10) |
| impurity phase fractions: h-FeSe, $\alpha$-Fe, $\gamma$-Fe, c-ZrO2 (wt %) | 9.11(12), 3.55(6), 5.18(9), 20.25(19) |
| goodness of fit, $wR_p$ (%), $R_p$ (%), $\chi^2$ | 1.04, 0.77, 4.167 |

The structural properties of the thin films were further investigated using Raman spectroscopy (Figure 3). The Raman measurements were carried out after only minimal exposure to air (*ca.* 5 s) and after 5 min of exposure in an effort to study any changes due to film oxidation. The $Fe_xZrSe_2$ films showed a minor scattering band at 173 $cm^{-1}$ and a major scattering band at 197 $cm^{-1}$, which were respectively consistent with the $E_g$ and $A_{1g}$ bands for $ZrSe_2$-like materials with $P\bar{3}m1$ symmetry.[30,42] No sign of the characteristic Raman bands for amorphous or crystalline $ZrO_2$[43] or $Fe_2O_3$[44,45] were detected from the 633 nm laser excitation.

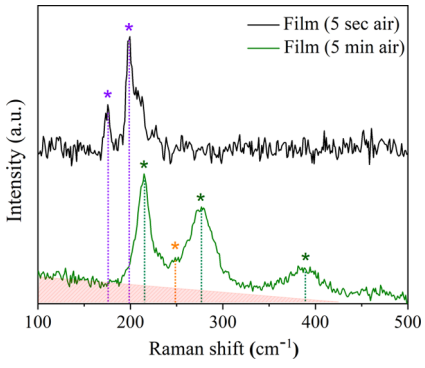


**Figure 3.** Raman spectra of the LPCVD grown $Fe_xZrSe_2$ films after minimal (*ca.* 5 s) and 5 min exposure to air. Bands corresponding to the contribution of $Fe_xZrSe_2$ (purple), iron oxide ($\alpha$-$Fe_2O_3$, green), selenium (Se, orange), and amorphous zirconia ($ZrO_2$, red) are detected in the spectra.

After exposure of the samples to air for 5 min, characteristic bands of $\alpha$-$Fe_2O_3$ were detected[44,45] together with a small contribution from amorphous selenium[46,47] (since the symmetric Se−Se stretching mode shows a very intensive Raman band, this spectrum indicates that the Se content is not very large). The uneven background in these spectra suggests the existence of amorphous $ZrO_2$ (red), which was also detected from XRD;[43] however, no $FeSe_x$ phases could be observed.[48,49]

X-ray photoelectron spectroscopy (XPS) was used to study the surface composition of the $Fe_xZrSe_2$ films. Zr, Se, Fe, and O were detected in the high-resolution XPS scans. The Zr 3d spectrum (Figure 4a) was fitted with a major doublet with the Zr $3d_{5/2}$ transition centered at 182.7 eV corresponding to Zr(IV) bound to Se or O and therefore providing evidence for the presence of $ZrSe_2$ and/or $ZrO_2$.[30,50] It has been previously reported that the intercalation of $ZrSe_2$ (Zr $3d_{3/2}$ = 183.05 eV) with a transition metal provokes a small shift of the Zr 3d environment to a lower energy (Zr $3d_{3/2}$ = 182.6 eV),[19] overlapping with the Zr environment from $ZrO_2$ (Zr $3d_{3/2}$ = 182.3 eV).[32] A further two minor sub-oxide environments were also found with the Zr $3d_{5/2}$ transitions at 178.6 and 180.3 eV.[50] The Se 3d spectrum (Figure 4b) was broad and best fitted with three sets of doublets with a $3d_{5/2}$-$3d_{3/2}$ separation of 0.86 eV. Se $3d_{5/2}$ peaks of almost equal intensity were found at 53.8 and 56.0 eV corresponding to $Se^{2-}$ bound to Zr and metallic Se ($Se^0$), respectively, therefore providing evidence for the $ZrSe_2$-based phase also seen from the XRD data as well as elemental selenium, a secondary product $ZrSe_2$ oxidation.[30,51] The third environment with the Se $3d_{5/2}$ peak at 59.5 eV matches with Se(IV) in the form of $SeO_2$, a possible native oxide product.[51] Fe was only detected with a low signal-to-noise ratio, and therefore the spectrum was not deconvoluted to determine oxidation states (see Supporting Information, Figure S3).

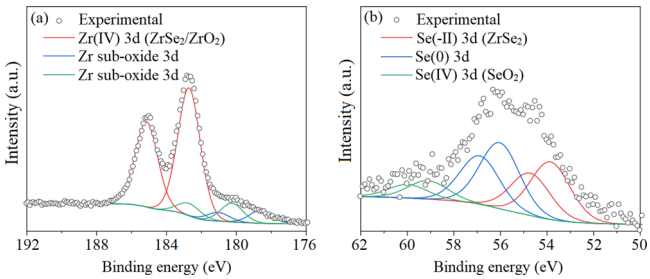


**Figure 4.** XPS data for a LPCVD grown $Fe_xZrSe_2$ film showing the (a) Zr 3d and (b) Se 3d transitions.

Compositional analysis of the surface of the film suggests a high excess of Se and O on the surface of the films relative to Zr (and Fe), suggesting surface segregation of the Se and native oxide formation, respectively. Depth profiling studies on a layer of ∼100 nm into the $Fe_xZrSe_2$ films revealed the total Fe-to-Zr ratio to be 0.12. It should be noted that the elemental composition calculations of O and Se were not carried out due


https://dx.doi.org/10.1021/acsomega.0c00413
ACS Omega XXXX, XXX, XXX−XXX

to the error associated with preferential sputtering of these lighter elements relative to Zr and Fe during the etching process.

The optical absorption spectrum of the $Fe_xZrSe_2$ thin film was calculated from sample transmittance and is shown in Figure 5 (black line). The direct optical band gap of the thin

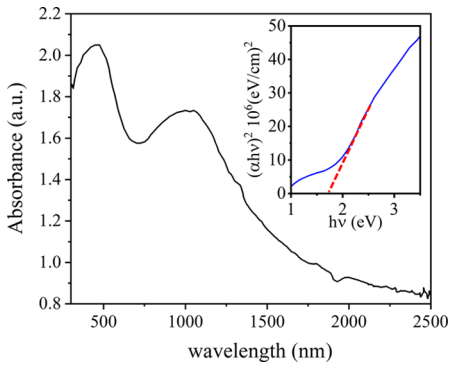


**Figure 5.** Absorbance (black line) of the thin film after minimal exposure to atmospheric conditions showing a $Fe_xZrSe_2$ absorption band centered at ~1000 nm and a second absorption band centered at ~450 nm due to the formation of $\alpha$-$Fe_2O_3$[52] upon exposure of the thin film to air prior to/during measurement. Graphical representation of band gap calculation using a Tauc plot is depicted in the inset.

film was determined plotting $(\alpha h\nu)^2$ against the photon energy ($h\nu$) (blue line) and extrapolating the linear part of the plot (broken red line). The obtained optical band gap value (1.72 eV) shows a small band gap increase (~0.2 eV) with respect to previously published values for $ZrSe_2$.[12,27,28]

## CONCLUSIONS

In conclusion, the formation of the $Fe_xZrSe_2$ ($x$ = 0.14) thin films *via* LPCVD from $[Fe(\eta^5\text{-}C_5H_4Se)_2Zr(\eta^5\text{-}C_5H_5)_2]_2$ was verified using PXRD, XPS, and Raman spectroscopy. The morphology of the thin films was evaluated using SEM and shown to consist of densely packed domes. Rietveld refinement analysis of PXRD data of the powder from film scrapping indicates the formation of a major phase of $Fe_xZrSe_2$ ($x$ = 0.14) and small impurity phases of Fe and FeSe presumably due to excess Fe plus post-deposition oxidation product $ZrO_2$. Raman bands show the expected $A_{1g}$ and $E_g$ modes for $Fe_xZrSe_2$ ($x$ = 0.14) ($CdI_2$ structure type, $P\bar{3}m1$). No bands for oxidation products were detected in freshly deposited films, whereas bands due to oxidation/decomposition products were found in films exposed to air for longer times. A small shift in the direct optical band gap was detected for $Fe_{0.14}ZrSe_2$ thin films with respect to the host material $ZrSe_2$. The extreme sensitivity of the $Fe_xZrSe_2$ materials requires a carefully designed and sealed setup for its synthesis, and therefore a single precursor offers better chances of homogeneity in the samples. Although utilization of the related precursor $[(^tBuSe)_2Se]$[31] could possibly be used for the synthesis of $Fe_xZrSe_2$ films in combination with an iron precursor, its higher toxicity and volatility makes its use far less desirable. Additionally, the selection of an oxygen-free iron source is not straightforward, as risk of carbon contamination can increase exponentially due to the increase of burned hydrocarbonated ligands and the use of alternative carbon-free sources (e.g., $FeCl_3$) could involve addition of undesired halogen doping. Although the proposed single-source precursor does not lead to a pure $Fe_xZrSe_2$ system using the described synthetic conditions, this study represents a proof of concept that the system can be synthesized from organometallic sources; the continuous development of organometallic sources with a variable ratio of Fe is extremely important for the future viability of these mixed metal selenides in industrial processes.

## EXPERIMENTAL SECTION

Precursors were synthesized according to literature procedures.[53] *N*,*N*,*N*′,*N*′-Tetramethylethylenediamine "TMEDA" (Aldrich) was distilled over sodium and stored over 3 Å molecular sieves (20% m/v) for 24 h. Ferrocene (Merck, 99%) was freeze-dried for 12 h prior to use. Selenium (shot, Aldrich), $^n$BuLi (2.5 M in hexane, Aldrich), and bis-(cyclopentadienyl)zirconium(IV) dichloride (Aldrich) were used as purchased. Dry tetrahydrofuran (99.9% in Argon, Sigma) and dry toluene were stored over a sodium mirror for 24 h prior to use, and pre-dried dichloromethane was dried over 3 Å molecular sieves (20% m/v) for 48 h prior to use. All preparations were undertaken using Schlenk techniques, and all glassware was dried for 12 h at 150 °C prior to use. The synthesis and purification of the precursor was performed under argon, which was passed over a drying column. After isolation, the polycrystalline powder precursor was stored in a glovebox under an argon atmosphere. Synthesis and purification of the precursor were confirmed by NMR and elemental analysis.[53] $[Fe(\eta^5\text{-}C_5H_4Se)_2Zr(\eta^5\text{-}C_5H_5)_2]_2$ (**1**): A bright red polycrystalline powder was isolated (1.25 g, 74%). $^1$H NMR (600 MHz) $\delta$/ppm ($C_6D_6$): 5.67 (s, 10H, Cp); 4.35 (m, 8H, Fc); $^{13}C\{^1H\}$ NMR (600 MHz) $\delta$/ppm ($C_6D_6$): 110.08 (m, Fc); 113.14 (m, Cp); $^{77}$Se NMR (400 MHz) $\delta$/ppm (tetrahydrofuran): 558.0; elemental analysis ($C_{40}H_{36}Se_4Fe_2Zr_2$): Calc. C, 42.64; H, 3.22. Found: C, 42.58; H, 3.35.

LPCVD experiments were carried out in a quartz tube under dynamic vacuum ($10^{-1}$ Torr) embedded inside a furnace to allow uniform heating, which was controlled using Pt−Rh thermocouples. The polycrystalline powder precursor (*ca.* 0.20 g) was spread evenly in a glazed aluminosilicate ceramic boat (0.9 × 1.4 × 10.3 cm, VWR cat. no. 459-0224) and heated up at 20 °C/min to 1000 °C and kept at that temperature for 1 h with the goal of achieving its sublimation over quartz slides (2.5 cm × 1.0 cm × 2 mm, Multi-Lab), which prior to use were cleaned using acetone (99%), isopropanol (99%), and distilled water and dried at 180 °C overnight. The method was followed by a gradual cooling process involving an initial cooling step of 13 °/min until reaching 355 °C followed by a second cooling step of 2 °C/min until reaching room temperature (switched off). The tube under vacuum was then transported inside a glovebox, where the films on both the quartz substrate and glazed aluminosilicate ceramic boat were stored for characterization. PXRD data were collected on a STOE diffractometer using monochromated $MoK_{\alpha1}$ radiation (0.70903 Å, 50 kV, 30 mA) and four scans per measurement over the 2$\theta$ range of 10−40°, with a step size of 0.5° and a count time of 10 s per step. Polycrystalline powders were ground in a metal mortar within the glovebox, loaded into sealed 3 mm borosilicate capillaries, and analyzed using a STOE Stadi P diffractometer ($MoK_{\alpha1}$ radiation, 0.70903 Å, 50 kV, 30 mA), in which less fluorescence was detected. Rietveld refinements were performed using GSAS and EXPGUI.[39] Raman spectroscopy of both powders and films was carried out using a Renishaw 1000 spectrometer equipped with a 633 nm laser. The Raman


https://dx.doi.org/10.1021/acsomega.0c00413
ACS Omega XXXX, XXX, XXX−XXX

system was calibrated using a silicon reference. X-ray photoelectron spectroscopy (XPS) of powders and films was performed using a Thermo K alpha spectrometer with monochromated $AlK_\alpha$ radiation (8.3418 Å), a dual beam charge compensation system, and a constant pass energy of 50 eV. Survey scans were collected in the range of 0−1200 eV. High-resolution peaks were used for the principal peaks of Zr (3d), Fe (2p), Se (3d), and C (1s). XPS data was analyzed using CasaXPS software, and the peaks were calibrated to adventitious carbon at 284.8 eV. Scanning electron microscopy (SEM) studies of film surfaces were carried out for thin film samples using JEOL 6301 (10 kV) and JEOL JSM-6700F field emission instruments after sputtering of the samples with a thin layer of gold to reduce charging. UV/Vis/near-IR transmission and reflection spectra were recorded in the range of 300−2500 nm using a Perkin-Elmer Fourier Transform Lambda 950 UV/Vis/NIR spectrometer. The transmission spectra background was taken against an air background, and a Labsphere reflectance standard was used as a reference material.

## ■ ASSOCIATED CONTENT

### Supporting Information

The Supporting Information is available free of charge at https://pubs.acs.org/doi/10.1021/acsomega.0c00413.

A table with the refined parameters for $Fe_xZrSe_2$ powder data, a high-quality image of the Rietveld refined powder data with the derived $Fe_xZrSe_2$ structure, and XPS survey and Fe surface scans of the thin film samples (PDF)

## ■ AUTHOR INFORMATION


### Corresponding Authors

**Risto S. Laitinen** − *Laboratory of Inorganic Chemistry, Environmental and Chemical Engineering, University of Oulu, Oulu FI-90014, Finland*; Email: risto.laitinen@oulu.fi

**Claire J. Carmalt** − *Materials Chemistry Centre, Department of Chemistry, University College London, London WC1H 0AJ, U.K.*; orcid.org/0000-0003-1788-6971; Email: c.j.carmalt@ucl.ac.uk

### Authors

**Clara Sanchez-Perez** − *Materials Chemistry Centre, Department of Chemistry, University College London, London WC1H 0AJ, U.K.; Laboratory of Inorganic Chemistry, Environmental and Chemical Engineering, University of Oulu, Oulu FI-90014, Finland*; orcid.org/0000-0003-3291-8601

**Caroline E. Knapp** − *Materials Chemistry Centre, Department of Chemistry, University College London, London WC1H 0AJ, U.K.*; orcid.org/0000-0003-4219-9313

**Ross H. Colman** − *Faculty of Mathematics and Physics, Charles University, Prague 2 121 16, Czech Republic*

**Carlos Sotelo-Vazquez** − *Materials Chemistry Centre, Department of Chemistry, University College London, London WC1H 0AJ, U.K.*; orcid.org/0000-0003-0949-4548

**Sanjayan Sathasivam** − *Materials Chemistry Centre, Department of Chemistry, University College London, London WC1H 0AJ, U.K.*; orcid.org/0000-0002-5206-9558

**Raija Oilunkaniemi** − *Laboratory of Inorganic Chemistry, Environmental and Chemical Engineering, University of Oulu, Oulu FI-90014, Finland*

Complete contact information is available at: https://pubs.acs.org/10.1021/acsomega.0c00413



### Funding

This work was supported by the Fortum Foundation, UCL, the Ramsay Memorial Trust, and EPSRC (grant EP/L017709).


### Notes

The authors declare no competing financial interest.

## ■ ACKNOWLEDGMENTS

Prof. Andrew L. Hector is thanked for his insightful comments. Dr. Steven Firth is thanked for useful discussions as well as training and assistance with the SEM instrument.

## ■ ABBREVIATIONS

TMDs, transition metal dichalcogenides; ITMDs, intercalated transition metal dichalcogenides; LPCVD, low-pressure chemical vapor deposition

## ■ REFERENCES


(1) Bhimanapati, G. R.; Lin, Z.; Meunier, V.; Jung, Y.; Cha, J.; Das, S.; Xiao, D.; Son, Y.; Strano, M. S.; Cooper, V. R.; Liang, L.; Louie, S. G.; Ringe, E.; Zhou, W.; Kim, S. S.; Naik, R. R.; Sumpter, B. G.; Terrones, H.; Xia, F.; Wang, Y.; Zhu, J.; Akinwande, D.; Alem, N.; Schuller, J. A.; Schaak, R. E.; Terrones, M.; Robinson, J. A. Recent Advances in Two-Dimensional Materials beyond Graphene. *ACS Nano* **2015**, *9*, 11509−11539.

(2) Wilson, J. A.; Yoffe, A. D. The Transition Metal Dichalcogenides Discussion and Interpretation of the Observed Optical, Electrical and Structural Properties. *Adv. Phys.* **1969**, *18*, 193−335.

(3) Yoffe, A. D. Electronic Properties of Low Dimensional Solids: The Physics and Chemistry of Layer Type Transition Metal Dichalcogenides and Their Intercalate Complexes. *Solid State Ionics* **1990**, *39*, 1−7.

(4) Marseglia, E. A. Transition Metal Dichalcogenides and Their Intercalates. *Int. Rev. Phys. Chem.* **2008**, *3*, 177−216.

(5) Friend, R. H.; Yoffe, A. D. Electronic Properties of Intercalation Complexes of the Transition Metal Dichalcogenides. *Adv. Phys.* **1987**, *36*, 1−94.

(6) Lee, P. A.; Said, G.; Davis, R.; Lim, T. H. On the Optical Properties of Some Layer Compounds. *J. Phys. Chem. Solids* **1969**, *30*, 2719−2729.

(7) Zheng, Y.; Wang, M.; Zhao, R.; Zhang, H.; Liu, D.; Li, D. Nonlinear Optical Absorption Properties of Zirconium Selenide in Generating Dark Soliton and Dark-Bright Soliton Pairs. *Appl. Opt.* **2020**, *59*, 396.

(8) Ōnuki, Y.; Inada, R.; Tanuma, S.-i.; Yamanaka, S.; Kamimura, H. Electrochemical Characteristics of $TiS_2$, $ZrSe_2$ and $VSe_2$ in Secondary Lithium Battery. *Jpn. J. Appl. Phys.* **1981**, *20*, 1583−1588.

(9) Ōnuki, Y.; Inada, R.; Tanuma, S.; Yamanaka, S.; Kamimura, H. Electrochemical Characteristics of $ZrSe_2$ in a Secondary Lithium Battery. *Solid State Ionics* **1983**, *8*, 141−145.

(10) Jiang, H. Structural and Electronic Properties of $ZrX_2$ and $HfX_2$ (X = S and Se) from First Principles Calculations. *J. Chem. Phys.* **2011**, *134*, 204705.

(11) Hankare, P. P.; Asabe, M. R.; Kokate, A. V.; Delekar, S. D.; Sathe, D. J.; Mulla, I. S.; Chougule, B. K. Effect of Annealing on Properties of ZrSe2 Thin Films. *J. Cryst. Growth* **2006**, *294*, 254−259.

(12) Moustafa, M.; Zandt, T.; Janowitz, C.; Manzke, R. Growth and Band Gap Determination of the $ZrS_xSe_{2-x}$ Single Crystal Series. *Phys. Rev. B* **2009**, *80*, No. 035206.

(13) Gleizes, A.; Revelli, J.; Ibers, J. A. Structures of a Semiconducting and a Metallic Phase in the $Fe_yZrSe_2$ System. *J. Solid State Chem.* **1976**, *17*, 363−372.

(14) Kang, M.; Rathi, S.; Lee, I.; Li, L.; Khan, M. A.; Lim, D.; Lee, Y.; Park, J.; Yun, S. J.; Youn, D.-H.; Jun, C.; Kim, G.-H. Tunable Electrical Properties of Multilayer $HfSe_2$ Field Effect Transistors by Oxygen Plasma Treatment. *Nanoscale* **2017**, *9*, 1645−1652.

(15) Buhannic, M.-A.; Ahouandjinou, A.; Danot, M.; Rouxel, J. Double coordinence du fer dans la phase $Fe_xZrSe_2$ ($0 < x < 0{,}25$): propriétés magnétiques et caractéristiques Mössbauer. *J. Solid State Chem.* **1983**, *49*, 77−84.
(16) Buhannic, M.; Danot, M. Iron Migration in the Van Der Waals Gap of Zirconium Disulfide: Time Evolution of the $FexZrS_2$ Compounds. *Solid State Commun.* **1990**, *73*, 739−742.
(17) Holgate, T. C.; Liu, Y.; Hitchcock, D.; Tritt, T. M.; He, J. Thermoelectric Properties of Li-Intercalated ZrSe2 Single Crystals. *J. Electron. Mater.* **2013**, *42*, 1751−1755.
(18) Titov, A. N.; Yagafarova, Z. A.; Bikkulova, N. N. Investigation into the Structural and Electrical Properties of Silver-Intercalated Zirconium Diselenide. *Phys. Solid State* **2003**, *45*, 2067−2071.
(19) Muhammad, Z.; Mu, K.; Lv, H.; Wu, C.; ur Rehman, Z.; Habib, M.; Sun, Z.; Wu, X.; Song, L. Electron Doping Induced Semiconductor to Metal Transitions in $ZrSe_2$ Layers via Copper Atomic Intercalation. *Nano Res.* **2018**, 4914.
(20) Ikhioya, L. I.; Chime, U. K.; Okoro, C. F.; Iroegbu, C.; Maaza, M.; Ezema, F. I. Influence of Dopant Concentration on the Electronic Band Gap Energy of Yb-$ZrSe_2$ Thin Films for Photovoltaic Application via Electrochemical Deposition Technique. *Mater. Res. Express* **2020**, *7*, No. 026420.
(21) Buhannic, M. A.; Colombet, P.; Danot, M. Spin-Glass Behavior of Iron-Intercalated Zirconium Disulfide. *Solid State Commun.* **1986**, *59*, 77−79.
(22) Fatseas, G. A.; Goodenough, J. B. Mössbauer $^{57}$Fe Spectra Exhibiting "Ferrous Character". *J. Solid State Chem.* **1980**, *33*, 219−232.
(23) McTaggart, F. K.; Wadsley, A. D. The Sulphides, Selenides, and Tellurides of Titanium, Zirconium, Hafnium, and Thorium. I. Preparation and Characterization. *Aust. J. Chem.* **1958**, *11*, 445.
(24) Greenaway, D. L.; Nitsche, R. Preparation and Optical Properties of Group IV−VI2 Chalcogenides Having the CdI2 Structure. *J. Phys. Chem. Solids* **1965**, *26*, 1445−1458.
(25) Vollath, D.; Szabó, D. V. Nanoparticles from Compounds with Layered Structures. *Acta Mater.* **2000**, *48*, 953−967.
(26) Berthier, C.; Chabre, Y.; Segransan, P.; Chevalier, P.; Trichet, L.; Le Mehaute, A. Semiconductor-Metal Transition upon Intercalation in $Li_xZrSe_2$. *Solid State Ionics* **1981**, *5*, 379−382.
(27) Asabe, M. R.; Ubale, V. P.; Rajmane, S. V.; Manukshete, A. H. Novel Route for Preparation of Zirconium Di-Selenide Thin Films. *DAV Int. J. Sci.* **2013**, *2*, 29.
(28) Sargar, A. M.; Patil, N. S.; Mane, S. R.; Gawale, S. N.; Bhosale, P. N. Electrochemical Synthesis and Characterisation of $ZrSe_2$ Thin Films. *Int. J. Electrochem. Sci.* **2009**, *4*, 87−894.
(29) Rakkini, A. P. V.; Mohanraj, K. Effect of Different Combinations of Precursors of Zirconium and Selenium in the Electrodeposited $ZrSe_2$ Thin Films. *Ionics* **2018**, *24*, 1243−1252.
(30) Tsipas, P.; Tsoutsou, D.; Marquez-Velasco, J.; Aretouli, K. E.; Xenogiannopoulou, E.; Vassalou, E.; Kordas, G.; Dimoulas, A. Epitaxial $ZrSe_2/MoSe_2$ Semiconductor v. d. Waals Heterostructures on Wide Band Gap AlN Substrates. *Microelectron. Eng.* **2015**, *147*, 269−272.
(31) Hector, A. L.; Levason, W.; Reid, G.; Reid, S. D.; Webster, M. Evaluation of Group 4 Metal Bis-Cyclopentadienyl Complexes with Selenolate and Tellurolate Ligands for CVD of $ME_2$ Films (E = Se or Te). *Chem. Mater.* **2008**, *20*, 5100−5106.
(32) Boscher, N. D.; Carmalt, C. J.; Parkin, I. P. Atmospheric pressure chemical vapor deposition of $WSe_2$ thin films on glass—highly hydrophobic sticky surfaces. *J. Mater. Chem.* **2006**, *16*, 122−127.
(33) Boscher, N. D.; Carmalt, C. J.; Parkin, I. P. Atmospheric Pressure CVD of $TiSe_2$ Thin Films on Glass. *Chem. Vap. Deposition* **2006**, *12*, 54−58.
(34) Sanchez-Perez, C.; Knapp, C. E.; Colman, R. H.; Sotelo-Vazquez, C.; Oilunkaniemi, R.; Laitinen, R. S.; Carmalt, C. J. Accessing New 2D Semiconductors with Optical Band Gap: Synthesis of Iron-Intercalated Titanium Diselenide Thin Films *via* LPCVD. *RSC Adv.* **2018**, *8*, 22552−22558.
(35) Kumar, R. S.; Zhang, Y.; Sinogeikin, S.; Xiao, Y.; Kumar, S.; Chow, P.; Cornelius, A. L.; Chen, C. Crystal and Electronic Structure of FeSe at High Pressure and Low Temperature. *J. Phys. Chem. B* **2010**, *114*, 12597−12606.
(36) Owen, E. A.; Yates, E. L. XLI. Precision Measurements of Crystal Parameters. *London Edinburgh Dublin Philos. Mag. J. Sci.* **2009**, *15*, 472−488.
(37) Basinski, Z. S.; Hume-Rothery, W.; Sutton, A. L. The Lattice Expansion of Iron. *Proc. R. Soc. London, Ser. A* **1955**, *229*, 459−467.
(38) Martin, U.; Boysen, H.; Frey, F. Neutron Powder Investigation of Tetragonal and Cubic Stabilized Zirconia, TZP and CSZ, at Temperatures up to 1400 K. *Acta Crystallogr., Sect. B: Struct. Sci., Cryst. Eng. Mater.* **1993**, *49*, 403−413.
(39) Larson, A. C.; Von Dreele, R. B. *GSAS*; 1985, The University of California: Los Alamos, NM, 87545.
(40) Momma, K.; Izumi, F. *VESTA 3* for Three-Dimensional Visualization of Crystal, Volumetric and Morphology Data. *J. Appl. Crystallogr.* **2011**, *44*, 1272−1276.
(41) Gleizes, A.; Jeannin, Y. Nonstoichiometry in the $ZrSe_2$ Phase. *J. Solid State Chem.* **1970**, *1*, 180−184.
(42) Mleczko, M. J.; Zhang, C.; Lee, H. R.; Kuo, H.-H.; Magyari-Köpe, B.; Moore, R. G.; Shen, Z.-X.; Fisher, I. R.; Nishi, Y.; Pop, E. $HfSe_2$ and $ZrSe_2$: Two-Dimensional Semiconductors with Native High-$\kappa$ Oxides. *Sci. Adv.* **2017**, *3*, No. e1700481.
(43) Tiseanu, C.; Cojocaru, B.; Parvulescu, V. I.; Sanchez-Dominguez, M.; Primus, P. A.; Boutonnet, M. Order and Disorder Effects in Nano-$ZrO_2$ Investigated by Micro-Raman and Spectrally and Temporarily Resolved Photoluminescence. *Phys. Chem. Chem. Phys.* **2012**, *14*, 12970.
(44) de Faria, D. L. A.; Venâncio Silva, S.; de Oliveira, M. T. Raman Microspectroscopy of Some Iron Oxides and Oxyhydroxides. *J. Raman Spectrosc.* **1998**, *28*, 873−878.
(45) Li, Y.-S.; Church, J. S.; Woodhead, A. L. Infrared and Raman Spectroscopic Studies on Iron Oxide Magnetic Nano-Particles and Their Surface Modifications. *J. Magn. Magn. Mater.* **2012**, *324*, 1543−1550.
(46) Yannopoulos, S. N.; Andrikopoulos, K. S. Raman Scattering Study on Structural and Dynamical Features of Noncrystalline Selenium. *J. Chem. Phys.* **2004**, *121*, 4747−4758.
(47) Goldan, A. H.; Li, C.; Pennycook, S. J.; Schneider, J.; Blom, A.; Zhao, W. Molecular Structure of Vapor-Deposited Amorphous Selenium. *J. Appl. Phys.* **2016**, *120*, 135101.
(48) Gnezdilov, V.; Pashkevich, Y. G.; Lemmens, P.; Wulferding, D.; Shevtsova, T.; Gusev, A.; Chareev, D.; Vasiliev, A. Interplay between Lattice and Spin States Degree of Freedom in the FeSe Superconductor: Dynamic Spin State Instabilities. *Phys. Rev. B* **2013**, *87*, 144508.
(49) Yuan, B.; Luan, W.; Tu, S.-t. One-Step Synthesis of Cubic $FeS_2$ and Flower-like $FeSe_2$ Particles by a Solvothermal Reduction Process. *Dalton Trans.* **2012**, *41*, 772−776.
(50) Tsunekawa, S.; Asami, K.; Ito, S.; Yashima, M.; Sugimoto, T. XPS Study of the Phase Transition in Pure Zirconium Oxide Nanocrystallites. *Appl. Surf. Sci.* **2005**, *252*, 1651−1656.
(51) Shenasa, M.; Sainkar, S.; Lichtman, D. XPS Study of Some Selected Selenium Compounds. *J. Electron Spectrosc. Relat. Phenom.* **1986**, *40*, 329−337.
(52) Wickman, B.; Bastos Fanta, A.; Burrows, A.; Hellman, A.; Wagner, J. B.; Iandolo, B. Iron Oxide Films Prepared by Rapid Thermal Processing for Solar Energy Conversion. *Sci. Rep.* **2017**, *7*, 40500.
(53) Sanchez-Perez, C.; Knapp, C. E.; Karjalainen, M. M.; Oilunkaniemi, R.; Carmalt, C. J.; Laitinen, R. S. Macrocycles Containing 1, 1'-Ferrocenyldiselenolato Ligands on Group 4 Metallocenes. *Dalton Trans.* **2018**, 5415.


https://dx.doi.org/10.1021/acsomega.0c00413
ACS Omega XXXX, XXX, XXX−XXX